

# Simulations of Overstable Inertial-acoustic Modes in Black-Hole Accretion Discs

Wen Fu<sup>1,2,3\*</sup> and Dong Lai<sup>1\*</sup>

<sup>1</sup>*Department of Astronomy, Cornell University, Ithaca, NY 14853, USA*

<sup>2</sup>*Theoretical Division, Los Alamos National Laboratory, Los Alamos, NM 87545, USA*

<sup>3</sup>*Department of Physics and Astronomy, Rice University, Houston, TX 77005, USA*

12 February 2018

## ABSTRACT

We present two-dimensional inviscid hydrodynamic simulations of overstable inertial-acoustic oscillation modes (p-modes) in black-hole accretion discs. These global spiral waves are trapped in the inner-most region of the disc, and are driven overstable by wave absorption at the corotation resonance ( $r_c$ ) when the gradient of the background disc vortensity (vorticity divided by surface density) at  $r_c$  is positive and the disc inner boundary is sufficiently reflective. Previous linear calculations have shown that the growth rates of these modes can be as high as 10% of the rotation frequency at the disc inner edge. We confirm these linear growth rates and the primary disc oscillation frequencies in our simulations when the mode amplitude undergoes exponential growth. We show that the mode growth saturates when the radial velocity perturbation becomes comparable to the disc sound speed. During the saturation stage, the primary disc oscillation frequency differs only slightly (by less than a few percent) from the linear mode frequency. Sharp features in the fluid velocity profiles at this stage suggest that the saturation results from nonlinear wave steepening and mode-mode interactions.

**Key words:** accretion, accretion discs – hydrodynamics – waves – instabilities – X-ray: binaries.

## 1 INTRODUCTION

In several recent papers (Lai & Tsang 2009; Tsang & Lai 2009c; Fu & Lai 2011; Horak & Lai 2013), we have presented detailed study of the linear instability of non-axisymmetric inertial-acoustic modes [also called p-modes; see Kato (2001) and Wagoner (2008) for review] trapped in the inner-most region of black-hole (BH) accretion discs. This global instability arises because of wave absorption at the corotation resonance (where the wave pattern rotation frequency matches the background disc rotation rate) and requires that the disc vortensity has a positive gradient at the corotation radius (see Narayan et al. 1987, Tsang & Lai 2008 and references therein). The disc vortensity (vorticity divided by surface density) is given by

$$\zeta = \frac{\kappa^2}{2\Omega\Sigma}, \quad (1)$$

where  $\Omega(r)$  is the disc rotation frequency,  $\kappa(r)$  is the radial epicyclic frequency and  $\Sigma(r)$  is the surface density<sup>1</sup>. General relativistic (GR) effect plays an important role in the instability: For a Newtonian disc, with  $\Omega = \kappa \propto r^{-3/2}$  and relatively flat  $\Sigma(r)$  profile, we have  $d\zeta/dr < 0$ , so the corotational wave absorption leads to mode damping. By contrast,  $\kappa$  is non-monotonic near a BH (e.g., for a Schwarzschild BH,  $\kappa$  reaches a maximum at  $r = 8GM/c^2$  and goes to zero at  $r_{\text{ISCO}} = 6GM/c^2$ ), the vortensity is also non-monotonic. Thus, p-modes with frequencies such that  $d\zeta/dr > 0$  at the corotation resonance are overstable. Our calculations based on several disc models and Paczynski-Witta pseudo-Newtonian potential (Lai & Tsang 2009, Tsang & Lai 2009c) and full GR (Horak & Lai 2013) showed that the lowest-order p-modes with  $m = 2, 3, 4, \dots$  have the largest growth rates, with the mode frequencies  $\omega \simeq \beta m \Omega_{\text{ISCO}}$  (thus giving commensurate frequency ratio  $2 : 3 : 4, \dots$ ), where the dimensionless constant  $\beta \lesssim 1$  depends weakly the disc prop-

\* Email: wenfu@astro.cornell.edu (WF); dong@astro.cornell.edu (DL)

<sup>1</sup> Equation (1) applies to barotropic discs in Newtonian (or pseudo-Newtonian) theory. See Tsang & Lai (2009c) for non-barotropic discs and Horak & Lai (2013) for full general relativistic expression.

erties. These overstable p-modes could potentially explain the High-frequency Quasi-Periodic Oscillations (HFQPOs) observed in BH X-ray binaries (e.g., Remillard & McClintock 2006; Belloni et al. 2012).

The effects of magnetic fields on the oscillation modes of BH accretion discs have been investigated by Fu & Lai (2009, 2011, 2012) and Yu & Lai (2013). Fu & Lai (2009) showed that the basic wave properties (e.g., propagation diagram) of p-modes are not strongly affected by disc magnetic fields, and it is likely that these p-modes are robust in the presence of disc turbulence (see Arras, Blaes & Turner 2006; Reynolds & Miller 2009). By contrast, other diskoseismic modes with vertical structure (such as g-modes and c-modes) may be easily “destroyed” by the magnetic field (Fu & Lai 2009) or suffer damping due to corotation resonance (Kato 2003; Li et al. 2003; Tsang & Lai 2009a). Although a modest toroidal disc magnetic field tends to reduce the growth rate of the p-mode (Fu & Lai 2011), a large-scale poloidal field can enhance the instability (Yu & Lai 2013; see Tagger & Pallet 1999; Tagger & Varniere 2006). The p-modes are also influenced by the magnetosphere that may exist inside the disc inner edge (Fu & Lai 2012).

So far our published works are based on linear analysis. While these are useful for identifying the key physics and issues, the nonlinear evolution and saturation of the mode growth can only be studied by numerical simulations. It is known that fluid perturbations near the corotation resonance are particularly prone to become nonlinear (e.g., Balmforth & Korycansky 2001; Ogilvie & Lubow 2003). Moreover, real accretion discs are more complex than any semi-analytic models considered in our previous works. Numerical MHD simulations (including GRMHD) are playing an increasingly important role in unraveling the nature of BH accretion flows (e.g., De Villiers & Hawley 2003; Machida & Matsumoto 2003; Fragile et al. 2007; Noble et al. 2009, 2011; Reynolds & Miller 2009; Beckwith et al. 2008, 2009; Moscibrodzka et al. 2009; Penna et al. 2010; Kulkarni et al. 2011; Hawley et al. 2011; O’Neill et al. 2011; Dolence et al. 2012; McKinney et al. 2012; Henisey et al. 2012). Despite much progress, global GRMHD simulations still lag far behind observations, and so far they have not revealed clear signs of HFQPOs that are directly comparable with the observations of BH X-ray binaries<sup>2</sup>. If the corotation instability and its magnetic counterparts studied in our recent papers play a role in HFQPOs, the length-scale involved would be small and a proper treatment of flow boundary conditions is important. It is necessary to carry out “controlled” numerical experiments to capture and evaluate these subtle effects.

In this paper, we use two-dimensional hydrodynamic

<sup>2</sup> Henisey et al. (2009, 2012) found evidence of excitation of wave modes in simulations of tilted BH accretion disks. Hydrodynamic simulations using  $\alpha$ -viscosity (Chan 2009; O’Neill et al. 2009) showed wave generation in the inner disk region by viscous instability (Kato 2001). The MHD simulations by O’Neill et al. (2011) revealed possible LFQPOs due to disk dynamo cycles. Dolence et al. (2012) reported transient QPOs in the numerical models of radiatively inefficient flows for Sgr A\*. McKinney et al. (2012) found QPO signatures associated with the interface between the disc inflow and the bulging jet magnetosphere (see Fu & Lai 2012). Note that the observed HFQPOs are much weaker than LFQPOs, therefore much more difficult to obtain by brute-force simulations.

simulations to investigate the nonlinear evolution of corotational instability of p-modes. Our 2D model has obvious limitations. For example it does not include disc magnetic field and turbulence. However, we emphasize that since the p-modes we are studying are 2D density waves with no vertical structure, their basic radial “shapes” and real frequencies may be qualitatively unaffected by the turbulence (see Arras et al. 2006; Reynolds & Miller 2009; Fu & Lai 2009). Indeed, several local simulations have indicated that density waves can propagate in the presence of MRI turbulence (Gardiner & Stone 2005; Fromang et al. 2007; Heinemann & Papaloizou 2009). Our goal here is to investigate the saturation of overstable p-modes and their nonlinear behaviours.

## 2 NUMERICAL SETUP

Our accretion disc is assumed to be inviscid and geometrically thin so that the hydrodynamical equations can be reduced to two-dimension with vertically integrated quantities. We adopt an isothermal equation of state throughout this study, i.e.  $P = c_s^2 \Sigma$  where  $P$  is the vertically integrated pressure,  $\Sigma$  is the surface density and  $c_s$  is the constant sound speed. Self-gravity and magnetic fields are neglected.

We use the Paczynski-Witta Pseudo-Newtonian potential (Paczynski & Witta 1980) to mimic the GR effect:

$$\Phi = -\frac{GM}{r - r_S}, \quad (2)$$

where  $r_S = 2GM/c^2$  is the Schwarzschild radius. The corresponding Keplerian rotation frequency and radial epicyclic frequency are

$$\Omega_K = \sqrt{\frac{GM}{r}} \frac{1}{r - r_S}, \quad (3)$$

$$\kappa = \Omega_K \sqrt{\frac{r - 3r_S}{r - r_S}}. \quad (4)$$

In our computation, we will adopt the units such that the inner disc radius (at the Inner-most Stable Circular Orbit or ISCO) is at  $r = 1.0$  and the Keplerian frequency at the ISCO is  $\Omega_{\text{ISCO}} = 1$ . In these units,  $r_S = 1/3$ , and

$$\Omega_K = \frac{2}{3} \frac{1}{r - r_S} \frac{1}{\sqrt{r}}. \quad (5)$$

Our computation domain extends from  $r = 1.0$  to  $r = 4.0$  in the radial direction and from  $\phi = 0$  to  $\phi = 2\pi$  in the azimuthal direction. We also use the Keplerian orbital period ( $T = 2\pi/\Omega_K = 2\pi$ ) at  $r = 1$  as the unit for time. The equilibrium state of the disk is axisymmetric. The surface density profile has a simple power-law form

$$\Sigma_0 = r^{-1}, \quad (6)$$

which leads to a positive vortensity gradient in the inner disc region. The equilibrium rotation frequency of the disc is given by

$$\Omega_0(r) = \sqrt{\frac{4/9}{r(r - 1/3)^2} - \frac{c_s^2}{r^2}}. \quad (7)$$

Throughout our simulation, we will adopt  $c_s = 0.1$  so that  $\Omega_0 \simeq \Omega_K$ .

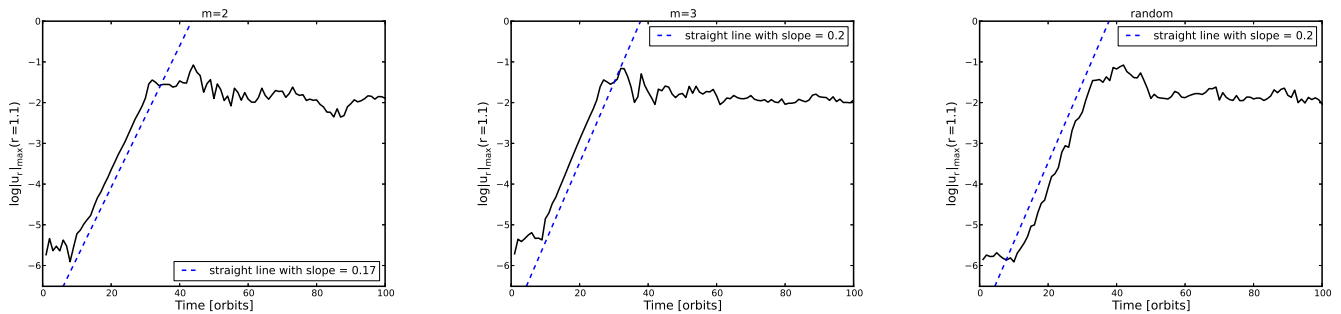


**Figure 1.** Evolution of the radial velocity amplitude  $|u_r|_{\max}$  (evaluated at  $r = 1.1$ ) for three runs with initial azimuthal mode number  $m = 2$  (left panel),  $m = 3$  (middle panel) and with random perturbations (right panel). The dashed lines are the fits for the exponential growth stage (between  $\sim 10$  and  $\sim 30$  orbits) of the mode amplitude.

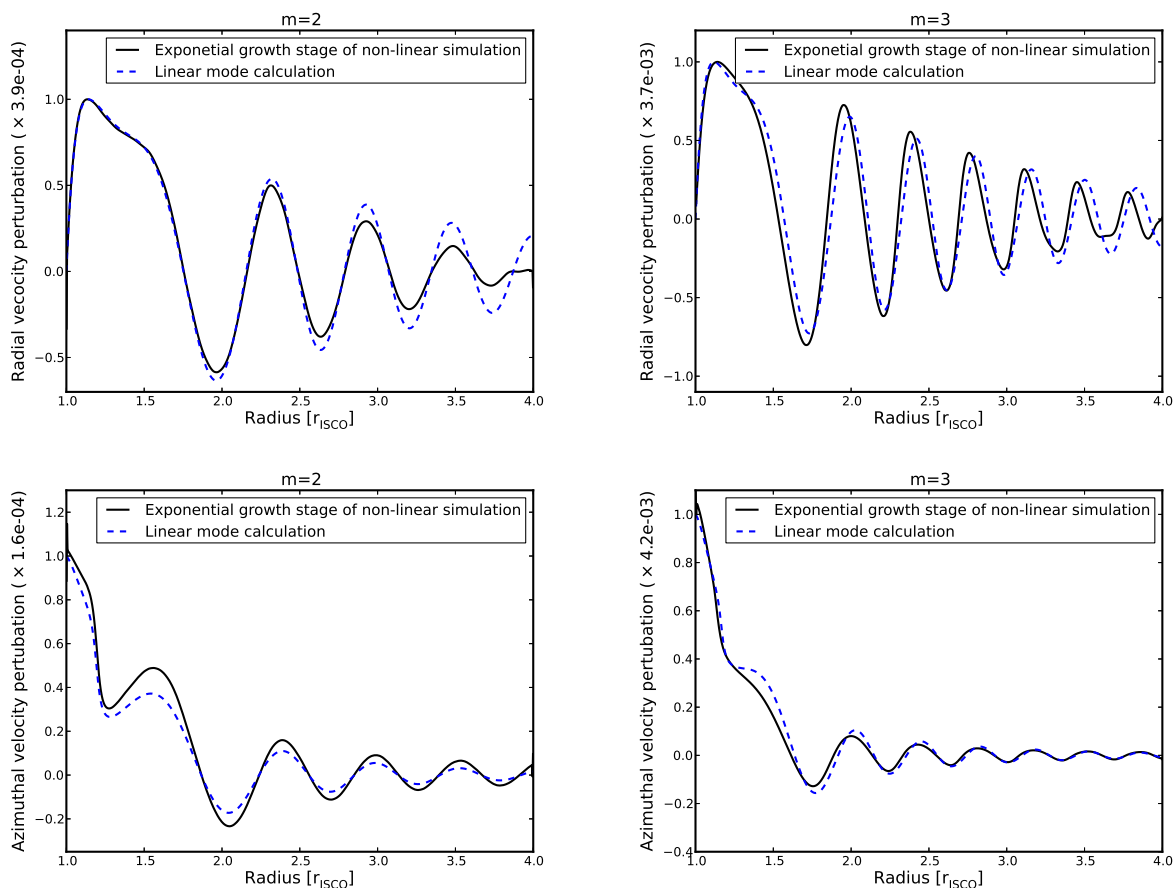


**Figure 2.** Comparison of the radial profiles of velocity perturbations from non-linear simulation and linear mode calculation. The top and bottom panels show the radial and azimuthal velocity perturbations, respectively. The left and right panels are for cases with azimuthal mode number  $m = 2$  and  $m = 3$ , respectively. In each panel, the dashed line is taken from the real part of the complex wavefunction obtained in linear mode calculation, while the solid line is from the non-linear simulation during the exponential growth stage (at  $T = 20$  orbits), with the quantities evaluated at  $\phi = 0.4\pi$ . Note that the normalization factor is given in the  $y$ -axis label for the nonlinear simulation results.

We solve the Euler equations that govern the dynamics of the disc flow with the PLUTO code<sup>3</sup> (Mignone et

al. 2007), which is a Godunov-type code with multiphysics and multialgorithm modules. For this study, we choose a Runge-Kutta scheme (for time integration) and piecewise linear reconstruction (for space integration) to achieve second order accuracy, and Roe solver as the solution of Rie-

<sup>3</sup> publicly available at <http://plutocode.ph.unito.it/>

mann problems. The grid resolution we adopt is  $(N_r \times N_\phi) = (1024 \times 2048)$  so that each grid cell is almost a square. Our runs typically last for 100 orbits (Keplerian orbits at inner disc boundary). To compare with the linear mode calculations (Lai & Tsang 2009), the inner disc boundary is set to be reflective with zero radial velocity. At the outer disc boundary, we adopt the non-reflective boundary condition. This is realized by employing the wave damping method (de Val-Borro et al. 2006) to reduce wave reflection. This implementation mimics the outgoing radiative boundary condition used in the linear analysis.

### 3 RESULTS

We carried out simulations with two different types of initial conditions for the surface density perturbation. In the first, we choose  $\delta\Sigma(r, \phi)$  to be randomly distributed in  $r$  and  $\phi$ . In the second, we impose  $\delta\Sigma(r, \phi) \propto \cos(m\phi)$  that is randomly distributed in  $r$ , so that the perturbation has an azimuthal mode number  $m$ . In all cases, the initial surface density perturbation has a small amplitude ( $|\delta\Sigma/\Sigma_0| \leq 10^{-4}$ ).

Fig. 1 shows the evolution of the radial velocity amplitude near the inner disc radius for runs with initial azimuthal mode number  $m = 2$ ,  $m = 3$  and random initial perturbation, respectively. This velocity amplitude is obtained by searching for the maximum  $|u_r|$  at a given  $r$  by varying  $\phi$  for each given time point. We chose  $r = 1.1$  because this is where the largest radial velocity perturbation is located (see the upper panels of Fig. 2). We see that in all cases there are three stages in the amplitude evolution. The first stage occupies roughly the first 10 orbits, during which the initial perturbation starts to affect the flow and presumably excites many modes/oscillations in the disc. In the second stage (from  $\sim 10$  orbits to  $\sim 30$  orbits), the fastest growing mode becomes dominant and undergoes exponential growth with its amplitude increased by about four orders of magnitude. In the last stage (beyond  $\sim 30$  orbits), the perturbation growth saturates and its amplitude remains at approximately the same level. A fit to the exponential growth stage gives the growth rate of the fastest growing perturbation, which is the slope of the fitted straight line. For the  $m = 2$  run, we find  $0.17/\log_{10}(e)/2\pi \simeq 0.0637$  (in units of the orbital frequency at  $r = 1$ ) as the growth rate, which is quite consistent with the result from our linear eigenmode calculation  $\omega_i \simeq 0.0632$  (the imaginary part of the eigenfrequency; Lai & Tsang 2009; Fu & Lai 2011; see Table 1). For the  $m = 3$  run, our simulation gives 0.074 as the mode growth rate, close to  $\omega_i = 0.0733$  from the linear calculation. In Fig. 2, we plot the radial profile of the velocity perturbation at a given time during the exponential growth stage of the simulation, and we compare it with the wavefunctions obtained from the linear mode calculation. Note that in each panel of Fig. 2 we have normalized the different sets of data so that they have the same scale. The normalization factor has also been included in figure labels for easy recovery of the absolute value in the simulation. We can see that wavefunctions obtained from two studies agree quite well. The only obvious differences are near the outer disc boundary, which can be attributed to the fact that outer boundary conditions employed in the numerical simulation and linear mode calculation are not exactly the same. Neverthe-

less, this agreement and the agreement in the mode growth rate in Fig. 1 confirm that our non-linear simulations indeed capture the same unstable disc p-modes as those revealed in linear perturbation analysis.

To explore the time variability of the flow, we carry out Fourier transform of the radial velocity  $u_r(r, \phi, t)$  at fixed  $r$  and  $\phi$  during different evolutionary stages. In Fig. 3 we show some examples of the resulting power density spectra (normalized to the maximum value of unity). Different rows correspond to different total sampling times and different columns represent runs with different initial surface density perturbation. In the left columns, the disk has an initial perturbation with azimuthal mode number  $m = 3$ . A mixture of various modes/oscillations are excited in the flow. After about 10 orbits of evolution, one of them (the fastest growing mode) has its oscillation amplitude grown by a large amount such that it dominates over other modes. This corresponds to the primary spike in the top-left panel. The other spikes in the same panel are harmonics of this primary spike (see the labels of the dashed vertical lines). Table 1 shows that the frequency<sup>4</sup> of this fastest growing mode ( $\omega_{r1}$ ) differs from the frequency obtained in linear mode calculation by only 0.3%, which again demonstrates the consistency of these two studies. After the perturbation saturates (bottom-left panel), we see that the basic structure of the power density spectrum does not change much except that these spikes are not as “clean” as in the linear regime; this is probably due to the interaction of different modes. Compared with the upper panel, the location of the primary spike ( $\omega_{r2}$  in Table 1) is increased by 2.0%. In Table 1 we also include the results from both linear mode calculation and numerical simulation for modes with other mode number  $m$ . The comparison illustrates two main points: First, the frequencies of the fastest growing modes during the exponentially growth stage of numerical simulations are exceptionally close to the linear calculation results (differ by less than 1%); second, the frequencies of the fastest growing modes during the saturation stage are only slightly higher (except for the  $m = 8$  mode which shows lower frequency) than ones during the exponential growing stage. These indicate that the mode frequencies obtained in linear mode calculation are fairly robust and can be reliably applied in the interpretation of HFQPOs.

In the right columns of Fig. 3, the simulation starts with a random initial perturbation which excites modes with various  $m$ 's. During the exponential growth stage, six modes stand out. By examining the location of the corresponding spikes, we know that these are the  $m = 3, 4, 5, 6, 7, 8$  modes. Although the  $m = 3$  mode seems to be the most prominent one in this figure, we note that this is because for this particular run the initial random perturbation happens to contain more  $m = 3$  wave components. If we were to start the run with a different initial random perturbation, then the relative strengths of those peaks would also be different (not necessarily with  $m = 3$  being dominant).

Fig. 4 shows the comparison of the velocity perturbations during the linear stage ( $T = 20$  orbits), at the end of the linear stage ( $T = 30$  orbits) and during the sat-

<sup>4</sup> All the frequencies in this paper are angular frequencies unless otherwise noted.

**Table 1.** Comparison of results from linear and nonlinear studies of overstable disc p-modes

$m^a$	$\omega_r^b$	$\omega_i^c$	$\omega_r/m\Omega^d$	$\omega_{r1}^e$	$ \omega_r - \omega_{r1} /\omega_r^f$	$\omega_{r2}^g$	$ \omega_{r2} - \omega_{r1} /\omega_{r2}^h$
2	1.4066	0.0632	0.7033	1.3998	0.5%	1.4296	2.1%
3	2.1942	0.0733	0.7314	2.1997	0.3%	2.2445	2.0%
4	3.0051	0.0763	0.7512	2.9996	0.2%	3.0594	2.0%
5	3.8294	0.0751	0.7659	3.7995	0.8%	3.8886	2.3%
6	4.6621	0.0714	0.7770	4.6494	0.3%	4.7749	2.6%
7	5.5007	0.0664	0.7858	5.4992	0.03%	5.6756	3.1%
8	6.3436	0.0607	0.7930	6.3492	0.09%	6.3189	0.5%

<sup>a</sup> Azimuthal mode number

<sup>b</sup> Mode frequency from the linear calculation (in units of Keplerian orbital frequency at the inner disc boundary; same for  $\omega_i$ ,  $\omega_{r1}$  and  $\omega_{r2}$ )

<sup>c</sup> Mode growth rate from the linear calculation

<sup>d</sup> Ratio of wave pattern speed to the Keplerian orbital frequency at the inner disc boundary

<sup>e</sup> Mode frequency during the exponential growth stage of nonlinear simulation (peak frequency of the power density spectrum between  $\sim 10$  orbits and  $\sim 30$  orbits)

<sup>f</sup> Difference between  $\omega_r$  (linear result) and  $\omega_{r1}$  (nonlinear result)

<sup>g</sup> Mode frequency during the saturation stage of nonlinear simulation (peak frequency of the power density spectrum between  $\sim 30$  orbits and  $\sim 100$  orbits)

<sup>h</sup> Difference between  $\omega_{r1}$  and  $\omega_{r2}$

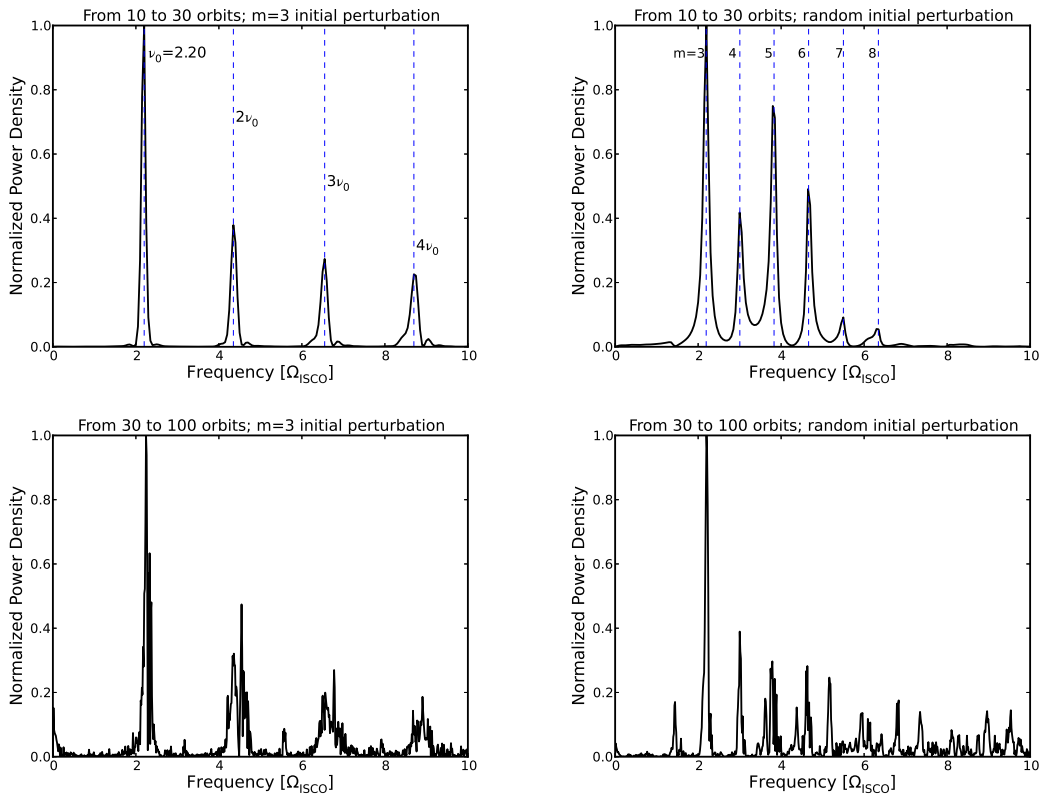


**Figure 3.** Power density spectra of the radial velocity perturbations near the disk inner boundary ( $r = 1.1$ ). Each panel shows the normalized FFT magnitude as a function of frequency. The left and right columns are for runs with initial  $m = 3$  and with random perturbation, respectively. In the top and bottom panels, the Fourier transforms are sampled for time periods of [10, 30] orbits and [30, 100] orbits, respectively.

uration stage ( $T = 50$  orbits) for simulations with different initial perturbations. At  $T = 20$  orbits, the oscillation mainly comes from the single fastest growing mode and has a smooth radial profile. At  $T = 30$  orbits, the perturbation starts to saturate, and the oscillation now consists of many different modes, and its radial profile exhibits sharp varia-

tions at several locations. These sharp features remain after the saturation ( $T = 50$  orbits).

To see this evolution from a different perspective, in Fig. 5 we show the color contours of radial velocity for runs with different initial perturbations (different columns) at different times (different rows). We can clearly see that spiral

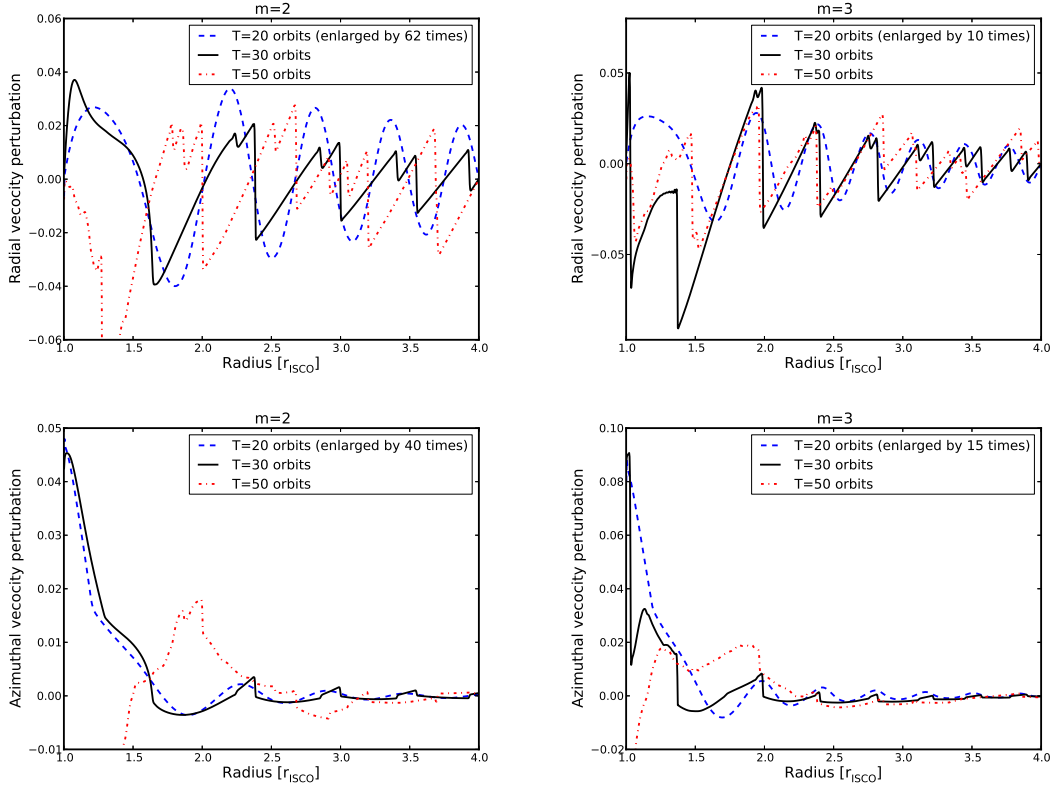


**Figure 4.** Evolution of the radial profiles of velocity perturbations from the non-linear simulations. The top and bottom panels show the radial and azimuthal components of velocity perturbation, respectively. The left and right panels are for cases with azimuthal mode number  $m = 2$  and  $m = 3$ , respectively. In each panel, the data are taken from points with fixed  $\phi = 0.4\pi$ . Different line types represent different times during the simulation.

waves gradually develop due to the instability. As the system evolves, sharp features in velocities emerge. At the end (the bottom row) the spiral arms becomes more irregular, which is related to the emergence and interaction of multiple modes after saturation.

The sharp velocity variations shown in Figs. 4-5 suggest shock-like features. Note that since our simulations adopt isothermal equation of state (with  $P/\Sigma = \text{constant}$ ), there is no entropy generation and shock formation in the strict sense. The radial velocity jump (see Fig. 4) is comparable but always smaller than the sound speed. Nevertheless, these sharp features imply that wave steepening plays an important role in the mode saturation.

## 4 CONCLUSIONS

We have carried out high-resolution, two-dimensional hydrodynamical simulations of overstable inertial-acoustic modes (p-modes) in BH accretion discs with various initial conditions. The evolution of disc p-modes exhibits two stages. During the first (linear) stage, the oscillation amplitude grows exponentially. In the cases with a specific azimuthal mode number ( $m$ ), the mode frequency, growth rate and wavefunctions agree well with those obtained in our previous linear mode analysis. In the cases with random initial perturbation, the disc power-density spectrum exhibits several prominent frequencies, consistent with those of the fastest

growing linear modes (with various  $m$ 's). These comparisons with the linear theory confirm the physics of corotational instability that drives disc p-modes presented in our previous studies (Lai & Tsang 2009; Tsang & Lai 2009c; Fu & Lai 2011, 2012). In the second stage, the mode growth saturates and the disc oscillation amplitude remains at roughly a constant level. In general, we find that the primary disc oscillation frequency (in the cases with specific initial  $m$ ) is larger than the linear mode frequency by less than 4%, indicating the robustness of disc oscillation frequency in the non-linear regime. Based on the sharp, shock-like features of fluid velocity profiles, we suggest that the nonlinear saturation of disc oscillations is caused by wave steepening and mode-mode interactions.

As noted in Section 1, our 2D hydrodynamical simulations presented in this paper do not capture various complexities (e.g., magnetic field, turbulence, radiation) associated with real BH accretion discs. Nevertheless, they demonstrate that under appropriate conditions, disc p-modes can grow to nonlinear amplitudes with well-defined frequencies that are similar to the linear mode frequencies. A number of issues must be addressed before we can apply our theory to the interpretation of HFQPOs. First, magnetic fields may play an important role in the disc oscillations. Indeed, we have shown in previous linear calculations (Fu & Lai 2011, 2012) that the growth of p-modes can be significantly affected by disc toroidal magnetic fields. A strong, large-



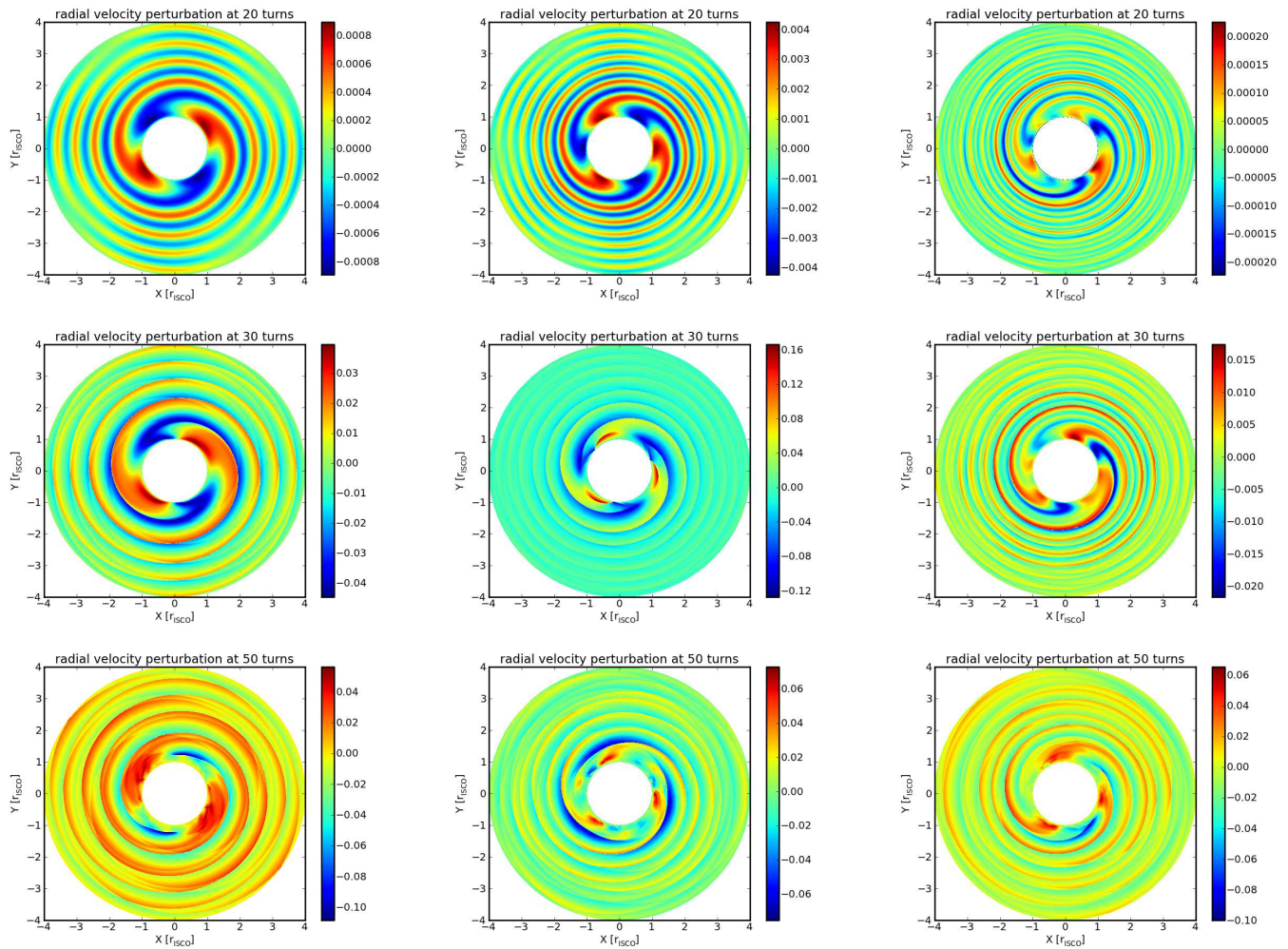


**Figure 5.** Evolution of the radial velocity for runs with initial  $m = 2$  (left),  $m = 3$  (middle) and random (right) perturbations, respectively. From top to bottom, the times are  $T = 20, 30$  and  $50$  orbits, respectively. Note that the color scale varies from panel to panel.

scale poloidal field can also change the linear mode frequency (Yu & Lai 2013). Whether or not these remain true in the non-linear regime is currently unclear. Second, understanding the nature of the inner disc boundary is crucial. Our calculations rely on the assumption that the inner disc edge is reflective to incoming spiral waves. In the standard disc model with zero-torque inner boundary condition, the radial inflow velocity is not negligible near the ISCO, and the flow goes through a transonic point. While the steep density and velocity gradients at the ISCO give rise to partial wave reflection (Lai & Tsang 2009), such radial inflow can lead to significant mode damping such that the net growth rates of p-modes become negative. This may explain the absence of HFQPOs in the thermal state of BH x-ray binaries. However, it is possible that the inner-most region of BH accretion discs accumulates significant magnetic flux and forms a magnetosphere. The disc-the magnetosphere boundary will be highly reflective, leading to the growth of disc oscillations (Fu & Lai 2012; see also Tsang & Lai 2009b). Finally, the effect of MRI-driven disc turbulence on the p-modes requires further understanding. In particular, turbulent viscosity may lead

to mode growth or damping, depending on the magnitude and the density-dependence of the viscosity (R. Miranda & D. Lai 2013, in prep).

#### ACKNOWLEDGEMENTS

This work has been supported in part by the NSF grants AST-1008245, AST-1211061 and the NASA grant NNX12AF85G. WF also acknowledges the support from the Laboratory Directed Research and Development Program at LANL.

#### REFERENCES

- Arras P., Blaes O. M., Turner N. J., 2006, *ApJ*, 645, L65  
 Balmforth N. J., Korycansky D. G. 2001, *MNRAS*, 326, 833  
 Beckwith K., Hawley J. F., Krolik J. H., 2008, *MNRAS*, 390, 21

- Beckwith K., Hawley J. F., Krolik J. H., 2009, *ApJ*, 707, 428
- Belloni T. M., Sanna A., Mendez M., 2012, *MNRAS*, 426, 1701
- Chan C.-K., 2009, *ApJ*, 704, 68
- de Val-Borro M., et al., 2006, *MNRAS*, 370, 529
- De Villiers J.-P., Hawley J. F., 2003, *ApJ*, 592, 1060
- Dolence, J.C., Gammie, C.F., Shiokawa, H., Noble, S.C. 2012, *ApJ*, 746, L10
- Fragile P. C., Blaes O., Anninos P., Salmonson J. D., 2007, *ApJ*, 668, 417
- Fromang S., Papaloizou, J., Lesur G., Heinemann T., 2007, *A&A*, 476, 1123
- Fu W., Lai D., 2009, *ApJ*, 690, 1386
- Fu W., Lai D., 2011, *MNRAS*, 410, 399
- Fu W., Lai D., 2012, *MNRAS*, 423, 831
- Gardiner T. A., Stone J. M., 2005, *AIP Conference Proceedings*, 784, 475
- Hawley J. F., Guan X., Krolik J. H., 2011, *ApJ*, 738, 84
- Heinemann T., Papaloizou J. C. B., 2009, *MNRAS*, 397, 52
- Henisey K. B., Blaes O. M., Fragile P. C., Ferreira B. T., 2009, *ApJ*, 706, 705
- Henisey K. B., Blaes O. M., Fragile P. C., 2012, *ApJ*, 761, 18
- Horak J., Lai D. 2013, *MNRAS*, in press
- Kato S., 2001, *PASJ*, 53, 1
- Kato S., 2003, *PASJ*, 55, 257
- Kulkarni A. K., et al., 2011, *MNRAS*, 414, 1183
- Lai D., Tsang D., 2009, *MNRAS*, 393, 979
- Li L., Goodman J., Narayan R., 2003, *ApJ*, 593, 980
- Machida M., Matsumoto R., 2003, *ApJ*, 585, 429
- McKinney J. C., Tchekhovskoy A., Blandford R. D., 2012, *MNRAS*, 423, 3083
- Mignone A., Bodo G., Massaglia S., Matsakos T., Tesileanu O., Zanni C., Ferrari A., 2007, *ApJS*, 170, 228
- Miranda R., Lai D., 2013, in preparation
- Moscibrodzka M., Gammie C. F., Dolence J. C., Shiokawa H., Leung Po Kin, 2009, *ApJ*, 706, 497
- Narayan R., Goldreich P., Goodman J., 1987, *MNRAS*, 228, 1
- Noble S. C., Krolik J. H., Hawley J. F., 2009, *ApJ*, 692, 411
- Noble S. C., Krolik J. H., Schnittman J. D., Hawley J. F., 2011, *ApJ*, 743, 115
- Ogilvie G. I., Lubow S. H., 2003, *ApJ*, 587, 398
- O'Neill S. M., Reynolds C. S., Miller C. M., 2009, *ApJ*, 693, 1100
- O'Neill S. M., Reynolds C. S., Miller C. M., Sorathia K., 2011, *ApJ*, 736, 107
- Paczynski B., Witta P. J., 1980, *A&A*, 88, 23
- Penna R. F., McKinney J. C., Narayan R., Tchekhovskoy A., Shafee R., McClintock J. E., 2010, *MNRAS*, 408, 752
- Remillard R. A., McClintock J. E., 2006, *ARA&A*, 44, 49
- Reynolds C. S., Miller M. C., 2009, *ApJ*, 692, 869
- Tagger M., Pellat R., 1999, *A&A*, 349, 1003
- Tagger M., Varniere P., 2006, *ApJ*, 652, 1457
- Tsang D., Lai D., 2008, *MNRAS*, 387, 446
- Tsang D., Lai D., 2009a, *MNRAS*, 393, 992
- Tsang D., Lai D., 2009b, *MNRAS*, 396, 589
- Tsang D., Lai D., 2009c, *MNRAS*, 400, 470
- Wagoner R. V., 2008, *J. Phys: Conf. Series*, Vol.118, 012006
- Yu C., Lai D., 2012, *MNRAS*, in press